ChemPubSoc Europe

DOI: 10.1002/chem.201701905

CHEMISTRY A European Journal Full Paper

Complex Chemistry

Stereochemical Alignment in Triphospha[3]ferrocenophanes

Stefan Borucki,[a] Zsolt Kelemen,[a] Martin Maurer,[a] Clemens Bruhn,[a] László Nyulászi,*[b] and Rudolf Pietschnig*[a]

Dedicated to Prof. Dr. Dr. h.c. mult. Evamarie Hey-Hawkins on the occasion of her 60th birthday

Abstract: A series of triphospha[3]ferrocenophanes of the type $Fe(C_5H_4\text{-}PtBu)_2PX$ with X = H, F, Cl, Br, I, NEt_2, *t*Bu has been prepared and characterized by heteronuclear NMR spectroscopy and X-ray crystallography. Despite having three stereogenic centers, the selective formation of a reduced number of diastereomers (either one or two) has been observed for these ferrocenophanes. Theoretical calculations revealed that the inversion of the central stereogenic center inverts the frontier orbital sequence leading to either an iron or a phosphorus centered HOMO depending on the respective diastereomer. CV measurements supported these results. For the all-*tert*-butyl substituted [3]ferrocenophane $Fe(C_5H_4)_2(PtBu)_3$ a chiral staggered conformation has been found in the solid state which differs substantially from the only other all-organo substituted [3]ferrocenophane, $Fe(C_5H_4)_2(PPh)_3$.

Introduction

[*n*]Ferrocenophanes, in which *n* atoms connect the two cyclopentadienyl rings within a ferrocene molecule, are attractive monomers for the ring opening polymerization (ROP) to ferrocenylene based polymers.[1] The ring strain present in ferrocenophanes with tight bridging units ($n = 1$) leads to structural peculiarities usually described as ring tilt which may involve direct interaction of the iron center with the bridging atom. For bridging units with $n = 2$, 3 some ring tilt may still be present but the tendency for thermal ROP is significantly reduced.[2] Despite the reduced ring strain the number of diphospha-[2]ferrocenophanes is scarce. The two phosphorus atoms in the bridge may occur as two pentavalent,[3] two trivalent,[2b,d] or a mixed situation with one trivalent connected to a pentavalent phosphorus atom.[2a] For triphospha[3]ferrocenophanes only two examples are known in the literature out of which only one has been structurally characterized.[2c,4] Since asymmetrically substituted phosphorus atoms act as stereogenic centers the number of diastereomers increases with the number of phosphorus atoms in a chain. Recently, we and others have demonstrated that the number of isomers can be reduced by embedding the phosphorus chain into a cyclic backbone[5] such as a ferrocenophane.[2a,6]

Encouraged by these findings we set out to explore the possibilities to prepare functionalized triphospha[3]ferrocenophanes and to explore their stereochemistry and reactivity with experimental and computational methods.

Results and Discussion

Synthesis of P-P-P [3]ferrocenophanes

A straightforward approach to P-P-P bridged [3]ferrocenophanes starts from secondary 1,1′-ferrocenylene bis(phosphanes) in which the bridging unit is closed by attachment of the central phosphanylidene unit as a cap. We selected bis(phosphane) **1** as starting point of this investigation because the *tert*-butyl groups should provide some steric protection and furthermore may serve as useful probe in ^1H NMR spectroscopy. Bis(secondary) phosphane **1** is readily prepared according to a published procedure and occurs as near 1:1 mixture of the *rac* and *meso* diastereomers owing to the presence of pairs of P-stereogenic centers.[6] Interestingly, the stereochemistry can be reset by lithiation with *n*BuLi affording dilithiophosphanide **2** in which both phosphorus atoms adopt a prochiral situation owing to the symmetric bridging of the two lithium atoms in solution as evident from multinuclear NMR spectroscopy in solution.[6] The identical $^1J_{(PLi)}$ coupling of 52 Hz from each lithium to both phosphorus nuclei is in agreement with related dimeric lithium and alkali phosphanides in the literature.[7]

[a] S. Borucki, Dr. Z. Kelemen, Dr. M. Maurer, Dr. C. Bruhn, Prof. Dr. R. Pietschnig
Institut für Chemie und CINSaT, Universität Kassel
Heinrich Plett-Straße 40
34132 Kassel (Germany)
E-mail: pietschnig@uni-kassel.de

[b] Prof. Dr. L. Nyulászi
Department of Inorganic and Analytical Chemistry
Budapest University of Technology and Economics
Szent Gellért tér 4, 1111 Budapest (Hungary)
E-mail: nyulaszi@mail.bme.hu

Supporting information for this article can be found under: https://doi.org/10.1002/chem.201701905.

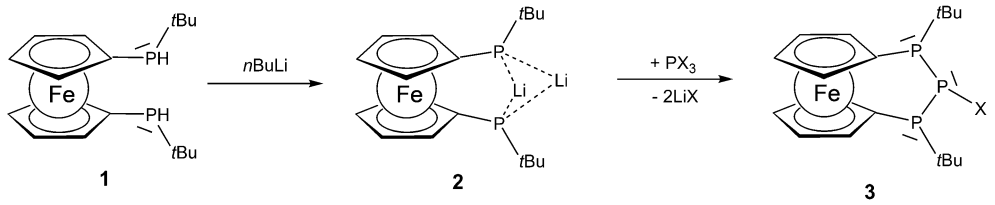

Scheme 1. Formation of [3]ferrocenophanes **3** (X = Cl (**3 b**), X = Br (**3 c**)).

During the reaction of dilithiated **2** with the trihalophosphanes PCl_3 and PBr_3 the envisaged [3]ferrocenophanes **3** are formed which entails the transformation of the prochiral phosphorus atoms to stereogenic centers (Scheme 1). In principle four diastereomers may be anticipated. In two of these diastereomers (A and B) the lone pairs of the cyclopentadienyl bonded phosphorus atoms are pointing to the same side of the ring while in case of C and D the lone pairs of these phosphorus atoms are oriented to opposite sides. A and B show either *cis* or *trans* orientation with respect to the central phosphorus atom (Figure 1) which entails maximized lone-pair interaction in A and minimized interaction in B. By contrast, only two adjacent phosphorus atoms of isomers C and D have the same orientation referring to the central ring.

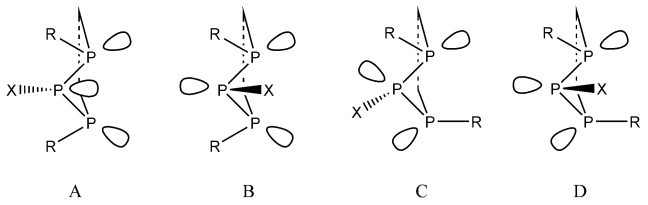

Figure 1. Schematic of the possible diastereomers with ferrocene omitted for clarity.

In the course of investigations only diastereomers A and B have been observed during the preparation of triphospha[3]-ferrocenophanes **3** as outlined in schemes 1 and 2. In general, these isomers show distinct differences in coupling constants related to the different interaction of the lone pairs for the *cis* and *trans* configuration (Table 1). Owing to the dependence of

Table 1. Survey of ^{31}P NMR data of compounds **3 a–d**.

X		Isomer A $\delta(^{31}P)$ [ppm]			Isomer B $\delta(^{31}P)$ [ppm]			Ratio
		P–X	P–*t*Bu	$^1J_{(PP)}$ [Hz]	P–X	P–*t*Bu	$^1J_{(PP)}$ [Hz]	A:B
F	**3 a**	247.2	15.0	359 357	–	–	–	100:0
Cl	**3 b**	147.7	18.2	377 372	61.8	4.2	170	59:41
Br	**3 c**	135.0	19.1	378 374	44.0	5.8	171	64:36
I	**3 d**	85.8	19.1	383 372	−3.5	10.2	169	60:40
H	**5**	−74.3	−9.8	295 289	−125.1	−6.5	107	42:58
NEt_2	**6**	–	–	–	70.0	−16.3	168	0:100
*t*Bu	**7**	–	–	–	46.2	−10.4 −10.3	357 356	0:100

$^1J_{(PP)}$ coupling constants on the dihedral angle,[8] isomers A reveal notable higher coupling constants for $^1J_{(PP)}$ than isomers B, since all lone pairs of A occupy a preferred gauche orientation. Moreover, the phosphorus chemical shifts are affected by the nature of the isomers. The resonances of isomers A experience a significant downfield shift of several tens of ppm in relation to isomers B.

As a typical example the ^{31}P NMR spectrum of **3 b** in solution is shown in Figure 2. The ^{31}P resonance of *cis*-**3 b** at 147.7 ppm indicates the presence of a chloro phosphane and the signal at 18.2 ppm lies in a typical region for *tert*-butyl substituted phosphanes. The $^1J_{(PP)}$ coupling pattern features a doublet of doublets for the >P–Cl fragment with coupling constants of 377 and 372 Hz. This indicates that the effective symmetry in solution is slightly lowered compared with the undistorted structure A of *cis*-**3 b** which may be attributed to the conformation-

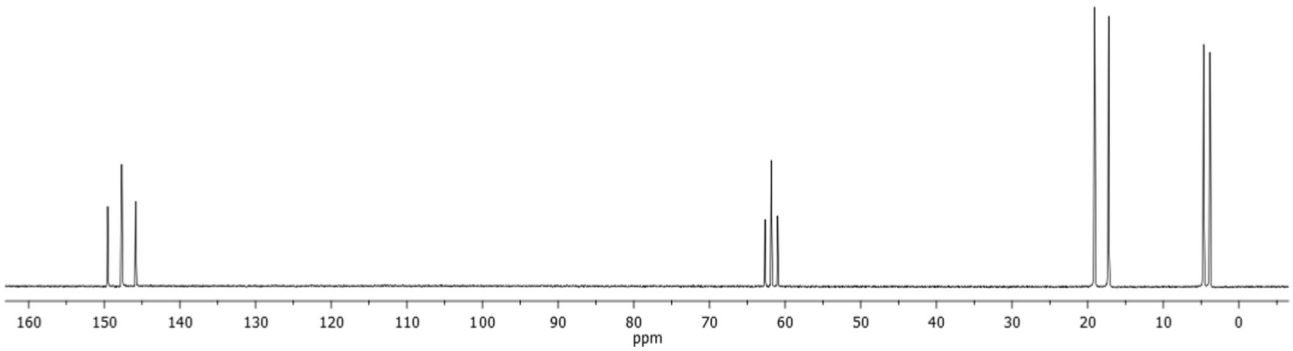

Figure 2. ^{31}P NMR spectrum of **3 b** in [D_6]benzene solution.

al flexibility of the adjacent ferrocene unit. The resonance of the related *tert*-butyl substituted phosphorus atoms show a pseudo doublet with a coupling constant of 375 Hz. The two anticipated doublets seem to have near identical chemical shifts and the shift difference is not resolved within the limits of signal linewidth. By contrast, the second set of signals originating from isomer *trans*-**3b** is shifted to higher field. Other than its *cis* isomer, *trans*-**3b** resonates as perfect triplet at 61.8 ppm for the >P–Cl fragment and as a doublet at 4.2 ppm for the *tert*-butyl substituted phosphorus atoms with a $^{1}J_{(PP)}$ coupling constant of 170 Hz.

Our DFT calculation revealed that isomer *cis*-**3b** is more stable than isomer *trans*-**3b** but the energy difference between them is small (2.0 kcal mol^{-1} at B3LYP/6–311+G** level of theory; Table S1 in the Supporting Information). We could locate a transition state of the interconversion of them, in which the inner >P–Cl phosphorus is planarized and the energy barrier of this process is 39.1 kcal mol^{-1} (Table S2 in the Supporting Information). In accordance with the high inversion barrier at phosphorus, which is even higher by a few kcal mol^{-1} than in the parent phosphane PH_3 (ca. 35 kcal mol^{-1}),[9] we did not observe any change in the *cis*–*trans* ratio by heating up the sample to 70 °C for 1 h. We have also computed the other two isomers (C and D), and also the transition structure for the inversion of the phosphorus at the >P–*t*Bu fragment which can give an alternative interconversion between A–B via C–D. These isomers exhibit lower stability (by 4.4 kcal mol^{-1} and 7.9 kcal mol^{-1}) than the most stable isomer A. Moreover, although the inversion barrier is also high (19.9 kcal mol^{-1} between isomers A and C and 25.6 kcal mol^{-1} between isomers B and D), it is still somewhat lower than the inversion barrier at the central phosphorus (39.1 kcal mol^{-1} between isomers A and B and 31.1 kcal mol^{-1} between isomers C and D). Earlier it has been demonstrated that phosphorus substitution at tricoordinate phosphorus decreases the inversion barrier substantially.[10] In full agreement with the experimental results the formation of C and D isomers are not favored both thermodynamically and kinetically.

Changing chlorine to bromine at the central phosphorus atom very similar NMR parameters are observed for compound **3c**. Both sets of signals for the *cis* and *trans* isomers of **3c** are shifted upfield in relation to **3b** but show almost the same $^{1}J_{(PP)}$ coupling constants. Isomer *cis*-**3c** resonates at 135.0 ppm as a doublet of doublets with coupling constants of 378 and 374 Hz and at 19.1 ppm as pseudo doublet with a pseudo coupling constant of 375 Hz. Isomer *trans*-**3c** reveals a triplet at 44.0 ppm and a doublet at 5.8 ppm with a coupling constant of 171 Hz. Similar to the chlorine analogue *trans*-**3c** is less stable by 2.0 kcal mol^{-1} than *cis*-**3c** (for the stability of the further possible isomers see Table S1 in the Supporting Information).

In order to check whether the preferred occurrence of isomers A and B is related to the prochiral nature of precursor **2** we also explored alternative synthetic approaches. The recently published bis(silylphosphane) **4** can be easily obtained as mixture of its *meso* and *rac* stereoisomers by silylation of **2**.[6] Bis(silylphosphane) **4** then reacts with the trihalophosphanes PCl_3 and PBr_3 eliminating trimethylsilyl halide at room temperature furnishing [3]ferrocenophanes **3** (Scheme 2). Interestingly, the same ratio of isomers A and B is obtained starting from stereochemically predefined precursors such as *rac*-/*meso*-**4** or prochiral **2**. Again no indication for the occurrence of isomers C and D has been found in using the silylphosphane route.

In an additional effort we explored the direct reaction of bis(secondary) phosphane **1** with trihalophosphanes in the presence of a base. Bis(phosphane) **1** undergoes the intended condensation reaction with PCl_3 or PBr_3 in pentane or hexane solution with an excess of triethylamine as base. The ammonium salt formed as by-product precipitates immediately upon addition of the trihalophosphane. The observed spectra are very clean and show only the formation of the desired product. Once again, only diastereomers A and B are formed de-

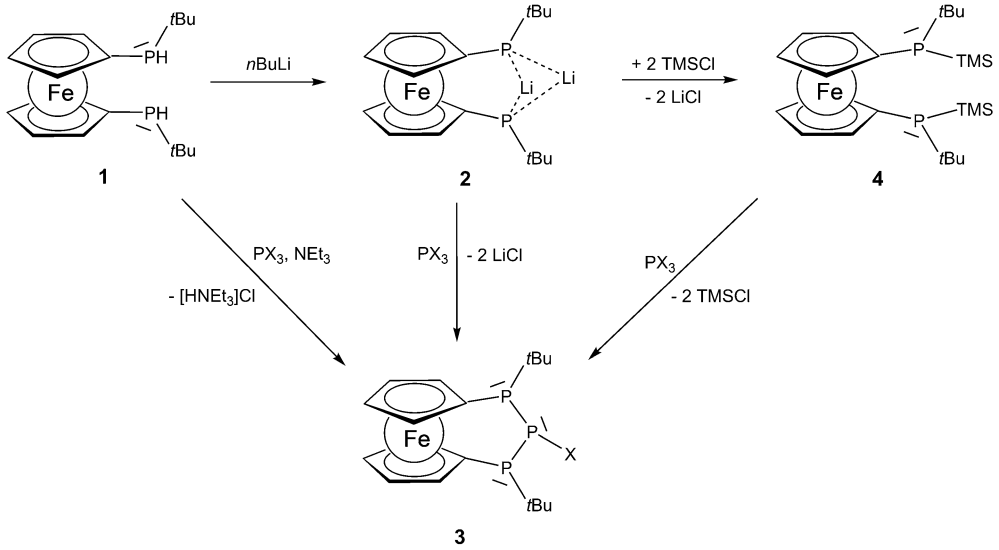

Scheme 2. Three different approaches for the formation of [3]ferrocenophane **3** starting from a diastereomeric mixture of bis(phosphane) **1** (X = Cl (**3b**), X = Br (**3c**)).

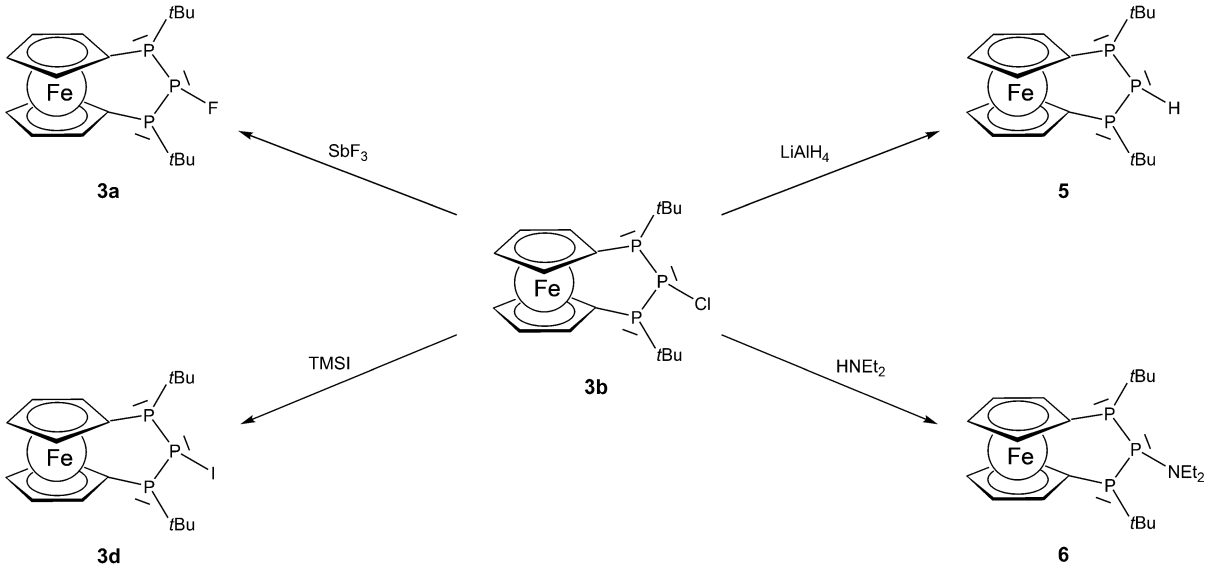

Scheme 3. Formation of **3a** and **3d** starting from chloro [3]Fc **3b** and reaction behavior towards reduction with $LiAlH_4$ and substituent exchange with diethylamine leading to **5** and **6**, respectively.

spite starting from stereochemically predefined **2** or from chiral mixture *rac*-/*meso*-**1**. As outlined above, we can synthesize [3]ferrocenophanes **3b**,**c** by three different approaches starting from bis(phosphane) **1** (Scheme 2). The base mediated condensation reaction represents the cleanest and most straight forward route with almost quantitative yields.

To complete the series of these functional [3]ferrocenophanes we also considered other halides at the central phosphorus atom. Iodophosphane **3d** can be prepared by halogen exchange reaction of chlorophosphane **3b** with trimethylsilyl iodide via elimination of the corresponding silyl chloride (Scheme 3). This method has some synthetic advantages compared with standard methods involving alkali metal iodides or magnesium iodide: reactions are running with mild conditions, easy to operate, rapid and can be run in different solvents.[11] It is known from the reactivity of trimethylsilyl iodide in the formation of phosphe(o)nium iodides that P–P cleavage may occur.[12] Owing to the presence of two P–P bonds in [3]ferrocenophane **3b**, side reactions limit the yield to about 40%. As expected the resulting by-products originate from P–P cleavage and one species could be identified as $Fe(C_5H_4PtBu)_2$. Nevertheless, **3d** could be purified and recrystallized and once again shows only the formation of isomers A and B with similar relative energy differences (1.7 kcal mol^{-1}) to **3b** and **3c** according to our DFT calculations. The ^{31}P NMR chemical shifts are the most shielded ones within the series of 2-halotriphospha[3]ferrocenophanes displaying a doublet of doublets at 85.8 ppm with $^1J_{(PP)}$ coupling constants of 383 and 372 Hz and a pseudo doublet at 19.1 ppm with a pseudo coupling constant of 378 Hz for isomer A. The set of signals for isomer B is even more shielded and exhibits a triplet at −3.5 ppm and a doublet at 10.2 ppm with coupling constants of 169 Hz.

Avoiding the gaseous and toxic phosphorus trifluoride, fluorophosphane **3a** was prepared using antimony trifluoride as fluorination reagent. Remarkably, the reaction of SbF_3 with **3b** in toluene at room temperature afforded only a single isomer of **3a**: the *cis* isomer A. The central fluoro substituted phosphorus atom is highly deshielded and resonates in the ^{31}P NMR spectrum at 247.2 ppm as doublet of doublets of doublets with a $^1J_{(PF)}$ coupling constant of 936 Hz and $^1J_{(PP)}$ coupling constants of 359 and 357 Hz. As with [3]ferrocenophanes **3b**, **3c** and **3d** the two doublets of the outer phosphorus atoms are not resolved and, therefore, display a pseudo doublet of doublets with a $^2J_{(PF)}$ coupling constant of 94 Hz and a pseudo $^1J_{(PP)}$ coupling constant of 358 Hz. The corresponding ^{19}F resonance of compound **3a** at −209.0 ppm shows a doublet of triplets with $^1J_{(FP)}$ and $^2J_{(FP)}$ coupling constants of 936 and 94 Hz, respectively.

The exclusive formation of *cis*-**3a** starting from *cis*-/*trans*-**3b** is remarkable and may be attributed to an S_N1 type mechanism with intermediate formation of the respective phosphenium cation (see the optimized structure and further information in the Supporting Information, Figure S1) which reacts with SbF_3Cl^- giving only the *cis*-**3a** isomer. Investigating the electrostatic potential map of the corresponding phosphenium cation (Figure S2 in the Supporting Information) it could be established that the front side (which leads to the *trans* isomer) of the central phosphorus atom is rather an electron rich area, thus any nucleophilic attack may occur at the other possible site, leading to the formation of the *cis* isomer. Furthermore *cis*-**3a**—similar to the other halogen analogues—exhibits somewhat higher (2.2 kcal mol^{-1}) stability. Further support to this surmise might come from the experimental observation of similar phosphenium cations.[13]

With the full series of 2-halotriphospha[3]ferrocenophanes in hand a clear trend can be derived from the ^{31}P NMR data (Table 1). With increasing electronegativity of the halide the central phosphorus nuclei is more deshielded while in turn the nuclei of the outer phosphorus atoms resonate at higher field. It is noteworthy that the influence of the halide on the chemi-

cal shift of the alkylated phosphorus nuclei is largest by switching from bromo to iodo substituted *trans*-**3** (isomer B). Furthermore, the central phosphorus nuclei of isomer *trans*-**3 d** is the most shielded one with a chemical shift below 0 ppm which is in line with the lower electronegativity of the iodo substituent. The values of the $^{1}J_{(PP)}$ coupling constants continuously increases with more electron density at the central phosphorus atom from F over Cl and Br to I substituted **3** in both isomers. The only exception is *trans*-**3 d** were the $^{1}J_{(PP)}$ value is lowest. Interestingly, the ratio of isomers in the case of **3 b**, **3 c** and **3 d** is not greatly affected by the size of the halide and lies around A:B = 60:40, and likewise the energy difference of the A and B isomers is small (1.8–2.2 kcal mol^{-1}).

Bonding situation in P-P-P [3]ferrocenophanes 3 a–d

For all triphospha[3]ferrocenophanes **3** single crystal structure analysis could be performed (Figures 3–6). All compounds show a unique stereochemical situation since both *tert*-butyl groups of the ring attached phosphanyl units point to the same side of the ring. As discussed above, **3 b**–**d** exhibit only the two isomers A and B in solution which differ from another by inversion of the central phosphanyl unit; **3 a** only shows isomer A. Consequently, the central phosphanyl unit is shifted to the same side as the *tert*-butyl groups irrespective of the position of the halide or isomer. It is noteworthy that bulky substituents (*t*Bu, NEt_2) at the P2 atom prefer the B structure.

All [3]ferrocenophanes represent almost unstrained structures with nearly eclipsed conformation of the ferrocene backbone (twist angles $\delta = 1.13^\circ$ (**3 a**), 2.47° (**3 b**), 6.52° (**3 c**), 0.49° (**3 d**)). The Cp-rings deviate slightly from coplanarity compared to ferrocene with interplanar angles α of 3.41° (**3 a**), 1.74° (**3 b**), 1.27° (**3 c**), and 2.88° (**3 d**).

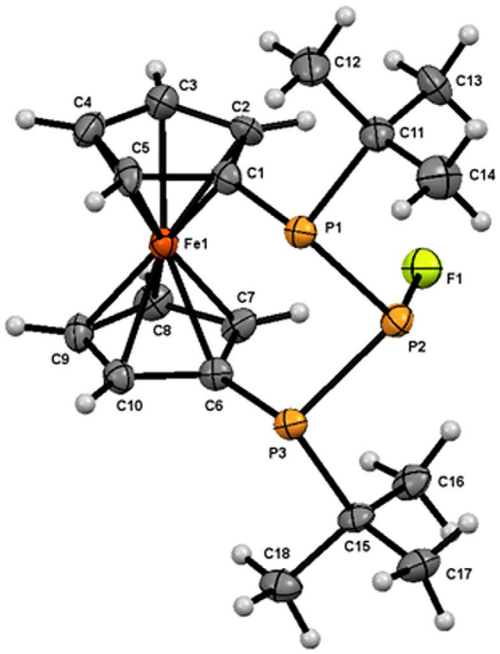

Figure 3. Molecular structure of **3 a**. Ellipsoids are drawn at 30% probability level.

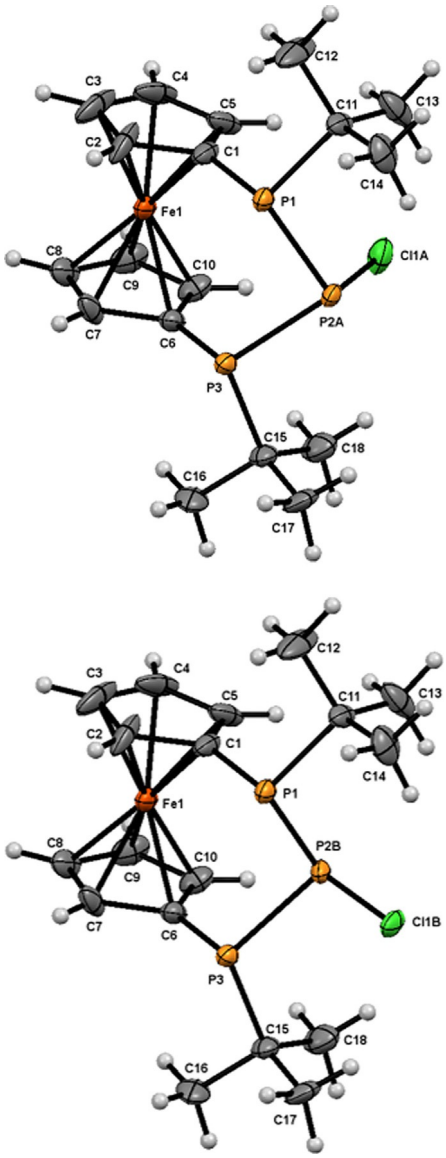

Figure 4. Molecular structure of isomers A (top) and B (bottom) of **3 b**. Ellipsoids are drawn at 30% probability level.

It needs to be mentioned that for **3 b** and **3 c** the asymmetric units contains both isomers resulting in disorder over two possible positions of the central phosphorus atom depending on the direction of the P–X bond. For **3 a** and **3 d** we observed only isomer A which is the major isomer in solution for all compounds (see Table 1). In contrary, the disordered crystals of **3 b** and **3 c** contain an inversed ratio of isomers in which isomer B is in the major component (A:B = approx. 40:60 (**3 b**), 25:75 (**3 c**)). Anyhow, the disorder in the crystal structures of **3 b** and **3 c** also limits the conclusions which can be drawn from the structural parameters related to the ferrocene backbone or *tert*-butyl groups. For the PPP scaffolds and the halides the atomic positions could be resolved, but all other atomic positions and derived parameters show large ellipsoids and high standard deviations. Interestingly, the *ipso* carbon atoms reveal comparatively small ellipsoids which suggests in turn that these positions are very similar in both isomers.

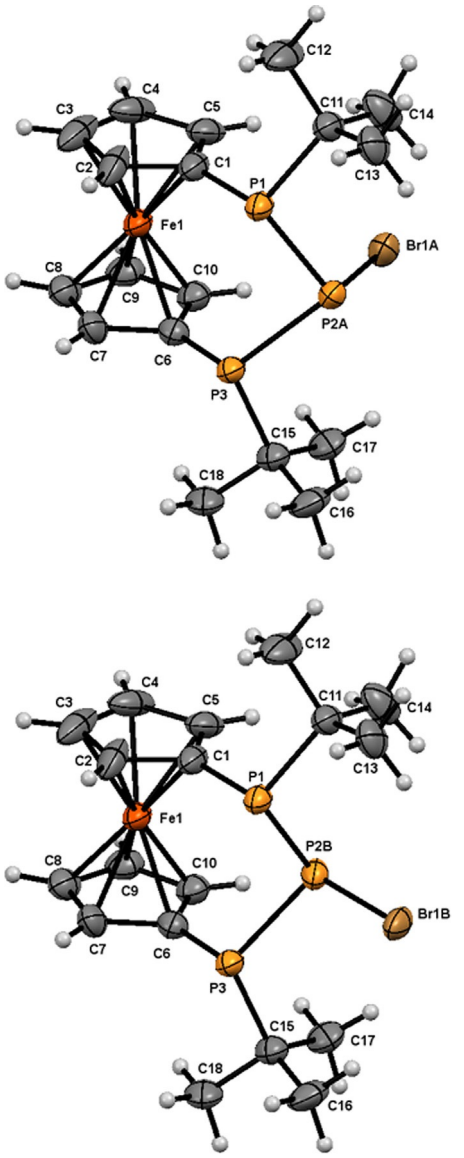

Figure 5. Molecular structure of isomers A (top) and B (bottom) of **3 c**. Ellipsoids are drawn at 30% probability level.

Within this series of compounds the ferrocene backbone is deformed due to the position of the halide in the *cis* isomer with most impact on carbons sites C3, C4, C8, and C9 (which show the biggest ellipsoids in **3 b** and **3 c**) and less on the *ipso* carbon sites. Therefore, a bending angle β can be defined which opens towards the side of the lone pairs and describes the deviation from linearity (5.44°/3.92° (**3 a**), 5.20°/6.89° (**3 b**), 6.03°/6.54° (**3 c**), 5.25°/5.14° (**3 d**)). With increasing size of the halide the PPP scaffold is shifted away from the iron center, widening the angles and slightly planarizing the phosphorus atoms which is indicated by the sum of angles at phosphorus (Table 2). This structural aspect in the solid state agrees nicely with the increasing $^{1}J_{(PP)}$ coupling values in solution on going from F to Cl and Br to I (see Table 1). Consequently, the distance between the iron center and the halide in *cis*-isomers increases within the same series (Table 3). It is striking that the Fe···P2 distance increases on going from the strongly electronegative F to Cl but then decreases going to the heavier halides.

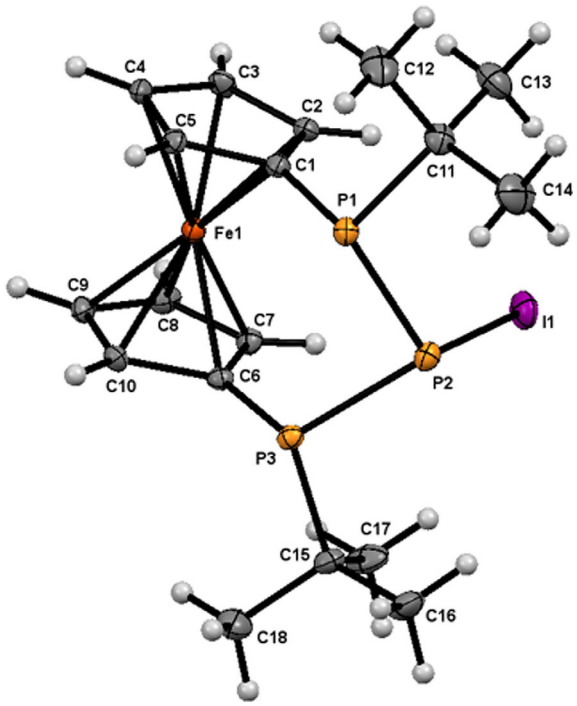

Figure 6. Molecular structure of isomer A of **3 d**. Ellipsoids are drawn at 30% probability level.

Table 2. Selected angles of compounds **3 a**–**d** and **5** [°]. With interplanar angle α, bending angle β (=180°–$\sphericalangle Cp_{centroid}$–$C_{ipso}$–P1 resp. P3), twist angle δ and the sum of angles Σ. Values marked with * limited interpretation possible owing to disorder over two positions.

X		α	β	δ	Isomer A Σ P1	Σ P2	Σ P3	$\sphericalangle$ Fe-P2-X	Isomer B Σ P1	Σ P2	Σ P3	$\sphericalangle$ Fe-P2-X
F	**3 a**	3.41	5.44 3.92	1.13	315.0(10)	308.4(5)	313.8(10)	72.1(2)	–	–	–	–
Cl	**3 b**	1.74*	5.20* 6.89*	2.47*	316.3(7)	312.0(6)	316.7(7)	79.4(2)	303.6(7)	288.8(6)	305.7(7)	157.0(2)
Br	**3 c**	1.27*	6.03* 6.54*	6.52*	317.5(11)	313.3(14)	317.1(11)	82.4(3)	303.1(8)	287.0(6)	303.2(7)	156.6(2)
I	**3 d**	2.88	5.25 5.14	0.49	322.7(4)	318.5(2)	322.7(4)	85.01(3)	–	–	–	–
H	**5**	3.96	5.94 5.80	5.69	310.0(4)	–	310.3(4)	–	–	–	–	–

Table 3. Selected distances of compounds **3a–d** and **5** [Å].

X		Isomer A P1–P2 P2–P3	P2–X	Fe–P2	Fe–X	Isomer B P1–P2 P2–P3	P2–X	Fe–P2
F	**3a**	2.189(4) 2.189(3)	1.612(4)	3.928(3)	3.760(5)	–	–	–
Cl	**3b**	2.252(5) 2.228(5)	2.095(7)	4.029(4)	4.185(3)	2.186(5) 2.187(4)	2.099(4)	3.552(3)
Br	**3c**	2.23(1) 2.27(1)	2.26(1)	4.07(1)	4.390(3)	2.217(4) 2.193(4)	2.271(4)	3.544(3)
I	**3d**	2.182(1) 2.182(2)	2.517(1)	4.047(1)	4.5766(8)	–	–	–
H	**5**	2.203(1) 2.206(1)	–	3.838(1)	–	–	–	–

Since we could not obtain diastereopure *trans*-[3]ferrocenophanes, it is only possible to compare the PPP scaffold found for **3b** and **3c**. The bond lengths and angles are without peculiarities and for all phosphorus atoms a more pyramidal structure can be derived for *trans*-**3b,c** compared with their *cis*-isomers. Especially P2 shows in both molecules *trans*-**3b,c** with 288.8(6)° and 287.0(6)° very low values for the sum of angles (280.8° PH_3).[14] This indicates a high s-character of the lone pair suggesting less interaction with the lone pairs of the Cp-bonded phosphorus atoms in agreement with lower $^1J_{(PP)}$ coupling constants (see Table 1). Also the inversion barrier was lower at this phosphorus atom. The halide atoms show an almost linear Fe···P2–X arrangement (157.0(2)° (**3b**) and 156.6(2)° (**3c**)) and accordingly the PPP scaffold is not shifted away from the iron center as in the *cis*-isomers. Consequently, the Fe···P2 distance shortens in the *trans*-isomers where the lone pair of P2 points towards the iron center.

In isomer B the bond angle sums are significantly smaller than in isomer A, approaching to the value in PH_3, which might be considered as "natural", since there is no steric strain. Thus, the B structure can be considered at first sight as less strained. Since, however, A is more stable than B, it seems that an extra stabilizing effect should act in that isomer, which overcomes the increased strain. Indeed, a second order perturbation theory analysis on the NBO basis reveals that in the A structure there are 7 kcal mol^{-1} stabilizing interactions between each of the lone pairs of the outer phosphoruses and the $\sigma_{P\text{-}Cl^*}$ orbital, while no similar stabilizing interaction occurs for the *trans* (B) structure.

In order to gain deeper insight into the electronic nature of the investigated **3a–d** compounds the energy and the shape of the frontier molecular orbitals were investigated. Figure 7 depicts the most important orbitals of *trans*-**3b** and *cis*-**3b** (for **3a**, **3c** and **3d** see Supplementary information Figures S4 and S5). While the LUMOs of both isomers are basically the phosphorus-chlorine antibonding σ*-orbital, the HOMOs exhibit significant differences. Albeit in case of *trans*-**3b** the lone pairs of the phosphorus have significant contribution to the HOMO, in case of *cis*-**3b** the HOMO is localized at the iron center (basically a *d*-orbital). At lower energy level (HOMO−1 in case of *trans*-**3b** and HOMO−3 for *cis*-**3b**) the analogous orbitals also exist. The stabilization of the lone pair orbitals in case of the A structure (*cis*), is in accordance with the above discussed interaction between the lone pairs of the outer phosphorus and the $\sigma_{P\text{–}Cl}$* unoccupied orbital. In accordance the LUMO (which has a significant $\sigma_{P\text{–}Cl}$* character) is also at higher energy for the *cis*-**3b** than for the *trans*-**3b**. A similar statement can be made for the other halogen analogues (see more detail in the Supporting Information). Clearly, these significant differences in the frontier orbitals predict different redox chemically behavior.

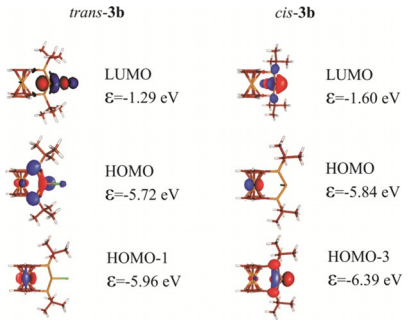

Figure 7. The most important Kohn–Sham orbitals of *trans*-**3b** and *cis*-**3b**.

Our cyclic voltammetric studies of chloro substituted **3b** and bromo substituted **3c** both show two irreversible electrochemical responses for the oxidation in dichloromethane (scan rate: 250 mV s^{-1}; **3b**: −0.03(1) V and +0.20(1) V vs. Fc/Fc$^+$; **3c**: +0.21(1) V and +0.72(1) V vs. Fc/Fc$^+$; Figure S6 in the Supporting Information). For **3b** several downstream processes can be observed reaching higher potentials over +0.5 V (vs. Fc/Fc$^+$). Since both compounds occur as stereochemical mixture of isomer A and B the two oxidation processes could be a superposition of *cis* and *trans* isomer—the energy levels of the HOMO are very similar—with follow up reaction of the generated cation. On the one hand, measurements with decreased scan rates down to 20 mV s^{-1}, giving the system time to react, revealed even less anodic current on the return for each redox process. On the other hand, if the potential was reduced after the first oxidation process the electrochemical response gets "more reversible" which could be confirmed by cyclic square wave voltammetry. Both experiments support the thesis of a follow up reaction. Due to the stereochemical mixture of **3b** and **3c**, the electrochemical mechanism could not be conclu-

sively clarified. It is known from the literature that substituents at ferrocene can render the corresponding ferrocenium species unstable. Increased scan rates may allow to prevent the decomposition of the monocation.[15]

Reactivity of X[3]Fc 3 b,c

Since we already started to explore the reactivity of halo triphospha[3]ferrocenophanes **3** by transforming **3 b** into **3 a** and **3 d**, respectively, we were interested in further investigating the reactivity of **3 b** and **3 c**.

The straightforward reduction of X[3]Fc **3 b**,**c** (X = Cl, Br) to the corresponding hydro triphospha[3]ferrocenophane **5** can be easily achieved by the reaction with lithium aluminum hydride (Scheme 3). As before, we only obtain two out of four possible isomers. As with [3]ferrocenophanes **3**, the *cis*-isomer A and *trans*-isomer B are displayed in the multinuclear NMR spectra. The $^{31}P\{^{1}H\}$ NMR spectrum features a doublet of doublets at −74.3 ppm for the phosphane fragment in *cis*-**5**. Different from **3** both corresponding doublets for the ring attached phosphorus atoms could be resolved with identical chemical shifts at −9.8 ppm and $^{1}J_{(PP)}$ coupling constants of 295 and 289 Hz, respectively. By contrast, the >P–H fragment of *trans*-**5** resonates as perfect triplet at higher field at −125.1 ppm and as doublet at −6.5 ppm for the alkylated phosphorus atoms with a $^{1}J_{(PP)}$ coupling constant of 107 Hz. It is conspicuous that the $^{1}J_{(PP)}$ coupling constants in both isomers of **5** are significantly lower compared with [3]ferrocenophanes **3**. Interestingly, the nature of the isomer does not influence the $^{1}J_{(PH)}$ coupling constant of the >P–H fragment (*cis*-**5**: 168 Hz; *trans*-**5**: 166 Hz) which produces a doublet of doublets of doublets (*cis*-**5**) respectively a doublet of triplets (*trans*-**5**) in the proton coupled phosphorus NMR spectrum. The corresponding signals in the ^{1}H NMR spectrum both feature a doublet of triplets originating from PP couplings to the direct bonded phosphorus atom and the two ring attached phosphorus atoms ($^{2}J_{(HP)}$ = 7 Hz (*cis*-**5**) and $^{2}J_{(HP)}$ = 8 Hz (*trans*-**5**)). Like the central phosphorus atom the proton of *cis*-**5** resonate at lower field (4.17 ppm) compared to *trans*-**5** (3.49 ppm). It has to be noted that the ratio of isomers in solution shows in fact an inverted situation of A:B = 42:58 compared to the halogenated species **3** (Table 1) and also isomer B exhibits somewhat larger stability (by 0.1 kcal mol^{-1}) according to our DFT calculation at B3LYP/6–311 + G** level of theory.

X-ray diffraction analysis on single crystals of **5** revealed the molecular structure of the compound in the solid state (Figure 8). The conformation of [3]ferrocenophane **5** is very similar to halogenated **3** (Table 2 and Table 3). With the proton as smallest possible substituent the deviation of the Cp-rings from coplanarity is largest in the series and the distortion of the ferrocene backbone is more distinct. Both observations eventually arise from more conformational flexibility and degrees of freedom due to lower steric pressure. Unfortunately, the proton of the central phosphane fragment could not be located on the Fourier map. A comparison with angles and bond lengths found for **3 a**–**d** suggests that the resolved structure demonstrates the *cis*-isomer of **5**. The sum of angles around

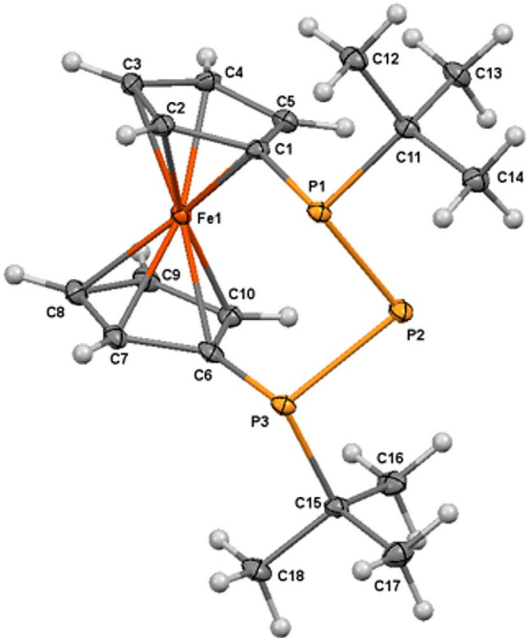

Figure 8. Molecular structure of **5**. The proton of the central >P–H fragment could not be located on the Fourier map. Ellipsoids are drawn at 30% probability level.

the ring attached phosphorus atoms and especially the Fe···P2 distance are in agreement with the series of substituents for isomer A (Tables 2 and 3). In tendency the sum of angles combined with the angle at the central phosphorus atom P1P2P3 = 91.68(5)° are smaller in *cis*-**5** compared with halogenated *cis*-**3** (**3 a**: 92.9(1)°, **3 b**: 92.2(2)°, **3 c**: 91.4(4)°, **3 d**: 92.34(6)°).

Multinuclear NMR analysis of crystals from **5** dissolved in [D_8]THF revealed a preferred crystallization of isomer A (*cis*-**5**:*trans*-**5** = 81:19). In the course of several days at room temperature the ratio of isomers returns again to A:B = 42:58 indicating a slow dynamic equilibrium in solution. The isomerization of *cis*-**5** to *trans*-**5** might proceed through inversion of the central >PH but the corresponding reaction barrier is high (31.2 kcal mol^{-1}), thus it is an unlikely mechanism at room temperature. Therefore, we have also considered the inversions of the two phosphorus atoms in the >P–*t*Bu fragment (via the formation of C type isomer as intermediate, see in Figure S3 in the Supporting Information). Although the inversion barriers of these steps are reduced (24.5–28.1 kcal mol^{-1}) compared to the direct conversion of the A and B isomers (31.2 kcal mol^{-1}), it is still a high value for a room temperature isomerization. In the view of these high barriers a deprotonation-protonation process might be a potential hypothesis.

So far all syntheses of PPP [3]ferrocenophanes outlined above led either to the formation of isomer A (only **3 a**) or a mixture of isomers A and B. With increasing size of the substituent at the central phosphanyl group an extent of steric pressure can be anticipated due to interaction with the ferrocene backbone as well as the two *t*Bu groups. This steric pressure is compensated by adaption of the bond angles of the

PPP scaffold as reflected by the sum of angles around P1 and P3 (Table 2). Thus, moving to bigger substituents should inhibit the formation of *cis*-isomer A, therefore we have chosen the NEt_2[16] and *t*Bu group. Our DFT calculations indicate an increased energy differences between isomers A and B (5.6 kcal mol^{-1} in case of NEt_2 and 3.8 kcal mol^{-1} for *t*Bu), which also predict the formation of isomer A over B.

A readily realized approach to introduce bulkier substituents at chloro phosphanes demonstrates the base mediated substitution reaction with secondary amines.[16] The substitution reaction of **3b** or **3c** with two equivalents diethylamine leads to the formation of the corresponding [3]ferrocenophane **6** (Scheme 3). ^{31}P NMR analysis indeed shows one set of signals indicating the formation of only one isomer of **6** alongside with a variety of side reaction products. Among these species we found the previously reported reduction product [2]ferrocenophane $Fe(C_5H_4PtBu)_2$[2b] and [3]ferrocenophane **5**. Amine substituted **6** or intermediates of the reaction mixture presumably undergo decomposition reactions with diethyl ammonium salt which is quantitatively formed by the condensation reaction of diethylamine and **3b** or **3c**, respectively, and is able to release the respective hydrogen halides. Starting from dilithiated **2** we can also synthesize **6** using Cl_2PNEt_2 in the absence of ammonium salt (Scheme 4). Applying this approach most of the side products can be avoided while $Fe(C_5H_4PtBu)_2$ is still present in the reaction mixture. Unfortunately, it could not fully separated from **6**.

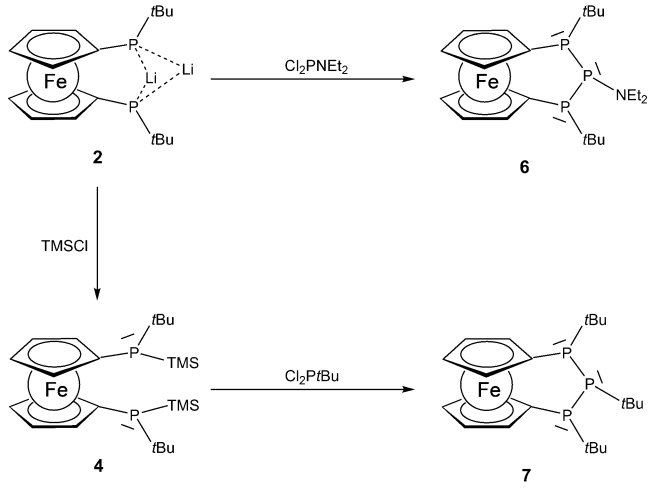

Scheme 4. Formation of [3]ferrocenophanes **6** and **7** starting from dilithiated **2**.

In the ^{31}P NMR spectra [3]ferrocenophane **6** occurs as triplet for the central $>P-NEt_2$ fragment with a chemical shift of 70.0 ppm featuring a $^1J_{(PP)}$ coupling constant of 168 Hz. The corresponding doublet resonates at −16.3 ppm. Matching these values with those found for [3]ferrocenophanes **3** and **5**, it is likely that the set of signals should arise from *trans*-isomer B which is in accordance with our expectations. Compared with *trans*-isomers **3b–d** the central phosphanyl group is deshielded and the ring attached phosphorus atoms are more shielded while the $^1J_{(PP)}$ coupling constant remains the same.

Now that we were able to synthesize compound **6** with only one isomer out of four we wondered whether it is possible to transform **6** back into corresponding chloro substituted **3b** maintaining or fully reverse the stereo information. As expected and mentioned before, treatment even with small amounts of hydrochloric acid leads to cleavage of the PP bonds generating starting compound **1** among several other species. On the contrary, PCl_3, which is known for scrambling reactions with amino substituted phosphanes[17] indeed principally forms [3]ferrocenophane **3b**. However, the stereo information gets lost in the course of reaction displaying again isomers A and B in NMR experiments.

In order to investigate the stereochemical consequence of a larger substituent at the central phosphorus atom, we set out to prepare an all-*tert*-butyl substituted PPP [3]ferrocenophane for which we anticipated the preferential formation of isomer B. While reaction of $tBuPCl_2$ with bis(secondary) phosphane **1** or its lithiated analogue **2** were unsuccessful, the envisaged formation was accomplished by the reaction of silylated **4** and $tBuPCl_2$ in boiling toluene (Scheme 4). After two days of reflux the starting materials are transformed into **7** in nearly quantitative yield and the product can be easily purified by recrystallization from diethylether.

In agreement with the occurrence of only a single diastereomer the all-*tert*-butyl substituted **7** shows only one set of signals in the ^{31}P NMR spectrum featuring a doublet of doublets at 46.2 ppm with coupling constants of 356 and 357 Hz, respectively. The two corresponding doublets resonate at −10.4 ppm and −10.3 ppm corroborating the inequivalence of the Cp-bonded phosphorus atoms. Despite this inequivalence the coupling pattern and the values for the coupling constants are rather close to those obtained for *cis*-**3**.

For the diasteropure [3]ferrocenophane **7** single crystal structure determination could be performed. The structure solution confirms that the *tert*-butyl groups of the central phosphanyl fragment and those of the ring attached phosphorus atoms point to different sides of the molecule (Figure 9). Therefore, we obtain a *trans*-like structure of the PPP bridge similar to isomer B, which exhibits higher stability than the corresponding **A** or **B** isomers by 5.8 and 9.6 kcal mol^{-1}, respectively.

Due to the bulky alkyl groups the whole structure is distorted to minimize repulsive interactions. Consequently, the ferrocene backbone has not longer a nearly ecliptic conformation but is twisted about 30.2°. The interplanar angle of 4.1° of the Cp ring planes now opens away from the bridge. As a result the former V-shaped phosphorus bridge changes to a helical structure. This also influences the positions of the outer *tert*-butyl groups, which have to be different due to the bond angle situation at the phosphorus atoms. One of the $P-C_{tBu}$ bonds opens a torsion angle of just 11.5(4)° while the second one exhibits a torsion angle of 58.0(4)° to the plane of the different Cp ring. It seems plausible to assume that the situation in solution can be inverted by rotation of the ferrocene backbone which results in a comparatively simple ^{31}P NMR spec-

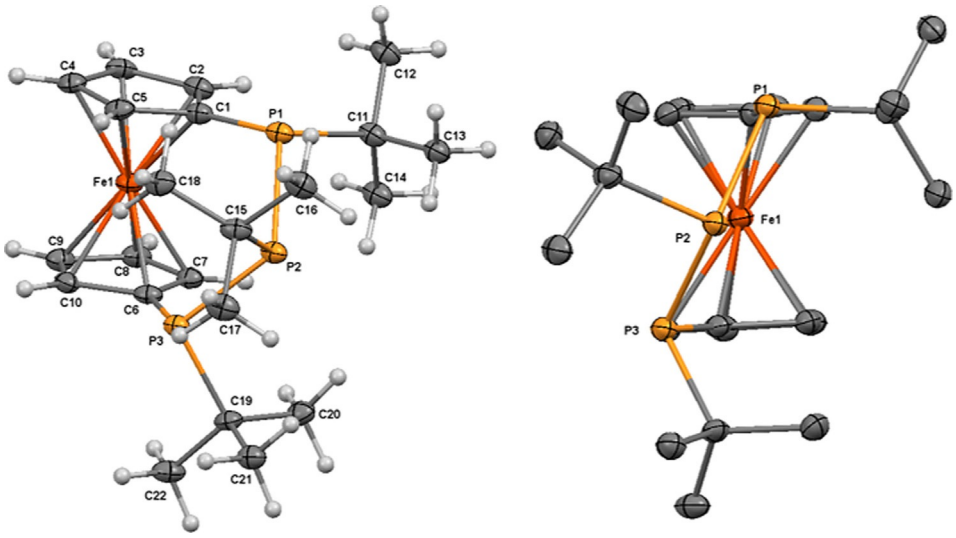

Figure 9. Molecular structure of **7** showing the steric congestion (left) and the distorted bridging unit with protons obmitted for clarity (right). Ellipsoids are drawn at 30% probability level. Selected bond lengths and angles of compounds **7**: interplanar angle $\alpha = 4.05^{\circ}$; bending angle β [$\hat{=} 180^{\circ} - \sphericalangle Cp_{centroid}–C_{ipso}–P1$ resp. P3] $= 7.56^{\circ}$ resp. 7.19°; twist angle $\delta = 30.22^{\circ}$; sum of angles: ΣP1 $= 322.5(4)^{\circ}$, ΣP2 $= 315.0(3)^{\circ}$, ΣP3 $= 313.8(4)^{\circ}$; bond lengths: P1–P2 = 2.207(1) Å, P2–P3 = 2.231(1) Å, P1–C_{tBu} = 1.887(4) Å, P3–C_{tBu} = 1.897(4) Å, P2–X = 1.903(4) Å, Fe–P2 = 4.113(1) Å.

trum. On a final note, the present steric pressure is also illustrated in the sum of angles for the phosphorus atoms which are comparable with those found for *cis*-**3 d**.

With this arrangement the molecular structure of **7** differs substantially from that of the only other all-organo substituted PPP [3]ferrocenophane published by Osborne et al. in the early 1990s, where the Cp-bonded phosphorus atoms share a mirror plane.[4] The unique situation in **7** corroborates the steric congestion exerted by the three neighboring *tert*-butyl groups leading to a relaxation with twisting about the ferrocene axis.

The electrochemical response of compound **7** should be more well-defined now that the compound consists of only one diastereomer and furthermore lacks reactive P–X bonds. Cyclic voltammetric measurements again reveal two distinct irreversible oxidation processes at +0.13(1) and +0.80(1) V (with 250 mV s^{-1}; vs. Fc/Fc^{+}; Figure S7 in the Supporting Information). Alike **3 b** and **3 c** the system gets more irreversible with lower scan rates. However, different from **3 b**,**c** both processes are more separated from each other (about 0.7 V at 250 mV s^{-1}; cf. about 0.2 V for **3 b** and ~0.5 V for **3 c**) and show well defined redox waves. Remarkably, with increasing scan rates the irreversible process converts over a quasi-reversible to a reversible redox process returning after the first oxidation. Since the HOMO of compound **7** contains contributions from both the iron center and the phosphorus lone pairs (Figure 10), it is still part of investigations whether the oxidation originates from the metal center or the bridging unit.

Compared with literature known [3]ferrocenophanes like the slightly electron-donating trimethylene bridged derivative $Fe(C_5H_4CH_2)_2CH_2$) (−0.07 V vs. Fc/Fc^{+})[18] and the electron-withdrawing trisulfur bridged analogue $Fe(C_5H_4S)_2S$ (+0.27 V vs. Fc/Fc^{+})[19] the all-*tert*-butyl triphospha[3]ferrocenophane (+0.13 V vs. Fc/Fc^{+}) is located right in the middle.

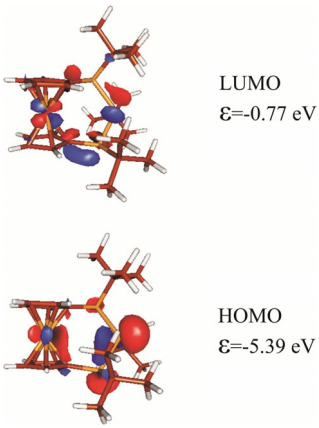

Figure 10. The most important Kohn–Sham orbitals of **7**.

Conclusion

In summary, we developed a general synthetic route to functional triphospha[3]ferrocenophanes for which stereochemical alignment depending on the substitution pattern has been achieved for a series of compounds **(3 a–d**, **5–7)**. While for most examples a mixture of isomers with *cis* and *trans* oriented vicinal substituents at phosphorus was observed, the exclusive formation of each of the *cis* or *trans* cases could be achieved by variation of the substituent pattern. The novel all-*tert*-butyl substituted [3]ferrocenophane **7** is only the second example of an all-organo substituted [3]ferrocenophane, and shows a completely different and moreover chiral structural motif in contrast to the previously known $Fe(C_5H_4PPh)_2PPh$. ^{31}P NMR proved to be an especially sensitive probe for the structural differences of the diastereomers observed in solution which are in good agreement with the solid state structures derived from X-ray crystallography. As a central part of our investigation, ab initio calculations have been performed which repro-

duce the structural peculiarities and moreover give insight into possible isomerization processes as well as the different electronic properties of the observed, as well as of the hypothetic, diastereomers. Most strikingly the inversion of the central phosphorus center, P2, affects the interaction σ_{P-X}* (X = Cl, Br) LUMO with the neighboring phosphorus lone pairs, stabilizing the occupied and destabilizing the unoccupied orbitals, changing the HOMO from an iron centered (in the *cis* isomer) to a phosphorus centered orbital (in the *trans* isomer). These theoretical findings were supported by electrochemical investigations which revealed irreversible processes for the diastereomeric mixtures, however are well resolved for compounds occurring as single isomers such as **7**. The latter results, moreover, hint at subsequent transformations occurring with rates in the range of the speed of the sweep voltage, which we would like to explore in the future with respect to radical formation and small molecule activation.

Experimental Section

All experiments were carried out under exclusion of moisture and air under an inert argon atmosphere. All solvents were dried over sodium potassium alloy and distilled prior to use. Starting materials were purified and stored under argon. $Fe(C_5H_4PHtBu)_2$ **1** was synthesized according to published procedures.[6] $PCl_2(NEt_2)$ is readily accessible using phosphorus trichloride and two equivalents of diethylamine and purification via distillation. *tert*-butyl dichlorophosphane ($tBuPCl_2$) was prepared reacting phosphorus trichloride with one equivalent of *tert*-butyllithium in pentane at −80 °C in quantitative yields. Subsequently, the resulting colorless liquid was purified via distillation to end up with a colorless solid. ^{1}H, ^{13}C, ^{19}F, and ^{31}P NMR spectra were recorded on a Varian VNMRS-500 MHz or MR-400 MHz spectrometer at room temperature using TMS as the external reference for ^{1}H and ^{13}C cores. Even for single crystalline samples microanalytic measurements resulted in too low carbon values suggesting metal carbide formation which could not be suppressed using standard additives such as V_2O_5. For all highly moisture and air sensitive compounds it was necessary to use EI-MS techniques for which we developed a method as inert as possible or were recorded via vAPCI-MS using iASAP on a Advion expressions CMS. Thus, for these compounds it was not possible to measure high resolution mass spectra. The APCI-MS spectrum for compound **7** has been recorded on a ThermoQuest Finnigan LCQ Deca.

Synthesis of 3 a

To a stirred suspension of 0.5 g (2.8 mmol) SbF_3 in 10 mL toluene a solution of 1.2 g (2.8 mmol) Cl[3]Fc **3 b** in 10 mL toluene were added dropwise at room temperature. After stirring overnight, all volatiles were removed in vacuo, extracted with 10 mL pentane and filtered off. The yellow crystalline product was obtained by crystallization at −20 °C from pentane. Yield: 0.7 g (60 %).

^{1}H NMR: (500 MHz, C_6D_6): δ = 1.29 (m, 18 H, *t*Bu CH_3), 3.96 (m, 2 H, Cp), 4.12 (m, 2 H, Cp), 4.48 (m, 2 H, Cp), 4.55 ppm (m, 2 H, Cp); ^{13}C NMR (126 MHz, C_6D_6): δ = 30.58 (m, *t*Bu CH_3), 32.29 (m, *t*Bu C_q), 69.64 (m, Cp), 72.90 (m, Cp), 76.19 (m, Cp), 78.27 (m, Cp C_{ipso}), 79.92 ppm (m, Cp); ^{19}F NMR (376 MHz, C_6D_6): δ = −209.0 ppm (dt, $^1J_{FP}$ = 936 Hz, $^2J_{FP}$ = 94 Hz); ^{31}P{^{1}H} NMR (202 MHz, C_6D_6): δ = 14.2 (dd, $^1J_{PP}$ = 358 Hz, $^2J_{PF}$ = 94 Hz, P–*t*Bu), 14.2 (dd, $^1J_{PP}$ = 358 Hz, $^2J_{PF}$ = 94 Hz, P–*t*Bu), 247.2 ppm (ddd, $^1J_{PF}$ = 936 Hz, $^1J_{PP}$ = 359 Hz, $^1J_{PP}$ = 357 Hz, P–F); MS (APCI) *m/z*: 411.0 (20 %, $[M+H]^+$), 363.1 (100 %, $[Fe(C_5H_4PHtBu)_2+H]^+$).

Synthesis of 3 b

To a stirred mixture of 2.37 g (6.5 mmol) $Fe(C_5H_4PHtBu)_2$ **1** and 3.7 mL (26.7 mmol) NEt_3 in 100 mL pentane 0.9 g (6.5 mmol) PCl_3 were added dropwise at room temperature. After continued stirring for 2 h, all volatiles were removed under reduced pressure. The residue was extracted with 20 mL pentane and filtered off. From the resulting orange solution the solvent was removed in vacuo yielding a yellow–orange crystalline solid which could be further purified by recrystallization from pentane at −20 °C. Yield: 2.7 g (97 %) crude product.

NMR spectra consist of signals from two diastereomers (*A* and *B*). ^{1}H NMR (400 MHz, C_6D_6): *A* δ = 1.30–1.35 (m, 18 H, *t*Bu CH_3), 3.93 (m, 2 H, Cp), 4.13 (m, 2 H, Cp), 4.47 (m, 2 H, Cp), 4.97 ppm (m, 2 H, Cp); *B* δ = 1.28–1.32 (m, 18 H, *t*Bu CH_3), 3.92 (m, 2 H, Cp), 3.95 (m, 2 H, Cp), 4.22 (m, 2 H, Cp), 4.29 ppm (m, 2 H, Cp); ^{13}C NMR (100 MHz, C_6D_6): *A* δ = 30.42 (m, *t*Bu CH_3), 33.64 (m, *t*Bu C_q), 69.56 (m, Cp), 72.94 (m, Cp), 76.12 (m, Cp), 79.44 (m, Cp C_{ipso}), 80.13 ppm (m, Cp); *B* δ = 30.09 (m, *t*Bu CH_3), 32.67 (m, *t*Bu C_q), 72.36 (m, Cp), 72.61 (s, Cp), 73.42 (m, Cp), 78.23 (m, Cp), 79.44 ppm (m, Cp C_{ipso}); ^{31}P{^{1}H} NMR (202 MHz, C_6D_6): *A* δ = 18.2 (d, $^1J_{PP}$ = 375 Hz, P–*t*Bu), 18.2 (d, $^1J_{PP}$ = 375 Hz, P–*t*Bu), 147.7 ppm (dd, $^1J_{PP}$ = 377 Hz, $^1J_{PP}$ = 372 Hz, P–Cl); *B* δ = 4.2 (d, $^1J_{PP}$ = 170 Hz, P–*t*Bu), 61.8 ppm (t, $^1J_{PP}$ = 170 Hz, P–Cl); MS (EI) *m/z*: 426.22 (30 %, M^+), 313.02 (100 %, $[M+H]^+-2\,t$Bu).

Synthesis of 3 c

To a stirred mixture of 0.83 g (2.3 mmol) $Fe(C_5H_4PHtBu)_2$ **1** and 0.9 mL (6.5 mmol) NEt_3 in 80 mL pentane 1.08 g (2.3 mmol) PBr_3 were added dropwise at room temperature. After continued stirring for 2 h, all volatiles were removed under reduced pressure. The residue was extracted with 20 mL pentane and filtered off. From the resulting yellow solution the solvent was removed in vacuo yielding a yellow crystalline solid which could be further purified by recrystallization from pentane at −20 °C. Yield: 0.98 g (90 %) crude product.

NMR spectra consist of signals from two diastereomers (*A* and *B*). ^{1}H NMR (400 MHz, C_6D_6): *A* δ = 1.29–1.36 (m, 18 H, *t*Bu CH_3), 3.93 (m, 2 H, Cp), 4.14 (m, 2 H, Cp), 4.45 (m, 2 H, Cp), 5.15 ppm (m, 2 H, Cp); *B* δ = 1.27–1.34 (m, 18 H, *t*Bu CH_3), 3.91 (m, 2 H, Cp), 3.95 (m, 2 H, Cp), 4.21 (m, 2 H, Cp), 4.27 ppm (m, 2 H, Cp); ^{13}C NMR (126 MHz, C_6D_6): *A* δ = 30.19–30.44 (m, *t*Bu CH_3), 34.01 (m, *t*Bu C_q), 69.74 (m, Cp), 72.71 (m, Cp), 75.00 (m, Cp), 79.54 (m, Cp C_{ipso}), 80.23 ppm (m, Cp); *B* δ = 30.17–30.31 (m, *t*Bu CH_3), 32.91 (m, *t*Bu C_q), 72.38 (m, Cp), 72.53 (m, Cp), 72.92 (m, Cp), 78.10 (m, Cp), 79.54 ppm (m, Cp C_{ipso}); ^{31}P{^{1}H} NMR (202 MHz, C_6D_6): *A* δ = 19.1 (d, $^1J_{PP}$ = 375 Hz, P–*t*Bu), 19.1 (d, $^1J_{PP}$ = 375 Hz, P–*t*Bu), 135.0 ppm (dd, $^1J_{PP}$ = 378 Hz, $^1J_{PP}$ = 374 Hz, P–Br); *B* δ = 5.8 (d, $^1J_{PP}$ = 171 Hz, P–*t*Bu), 44.0 ppm (t, $^1J_{PP}$ = 171 Hz, P–Br); MS (EI) *m/z*: 469.82 (8 %, M^+), 412.74 (5 %, M^+-tBu), 356.72 (23 %, $[M+H]^+-2t$Bu), 56.89 (100 %, tBu$^+$).

Synthesis of 3 d

0.44 g (1.0 mmol) Cl[3]Fc **3 b** were stirred in 30 mL pentane at room temperature. To this solution 0.21 g (1.0 mmol) TMSI were added dropwise and stirring was continued for 40 h at room temperature. From the resulting red solution all volatiles were removed under reduced pressure. The residue was recrystallized

from pentane at −20 °C affording the product as bright red needles. Yield: 0.21 g (40 %).

NMR spectra consist of signals from two diastereomers (*A* and *B*). ^{1}H NMR (500 MHz, C_6D_6): *A* δ = 1.28 (m, 18 H, *t*Bu CH_3), 3.92 (m, 2 H, Cp), 4.17 (m, 2 H, Cp), 4.44 (m, 2 H, Cp), 5.38 ppm (m, 2 H, Cp); *B* δ = 1.36 (m, 18 H, *t*Bu CH_3), 3.89 (m, 2 H, Cp), 3.96 (m, 2 H, Cp), 4.23 (m, 2 H, Cp), 4.26 ppm (m, 2 H, Cp); ^{13}C NMR (126 MHz, C_6D_6): *A* δ = 29.99 (m, *t*Bu CH_3), 34.07 (m, *t*Bu C_q), 69.94 (m, Cp), 71.99 (m, Cp), 72.11 (m, Cp), 78.56 (m, Cp C_{ipso}), 80.59 ppm (m, Cp); *B* δ = 30.54 (m, *t*Bu CH_3), 33.16 (m, *t*Bu C_q), 71.93 (m, Cp), 72.18 (m, Cp), 72.30 (m, Cp), 78.06 (m, Cp), 78.56 ppm (m, Cp C_{ipso}); ^{31}P{^{1}H} NMR (202 MHz, C_6D_6): *A* δ = 19.1 (d, $^{1}J_{PP}$ = 378 Hz, 2 P–*t*Bu), 19.1 (d, $^{1}J_{PP}$ = 378 Hz, 2 P–*t*Bu), 85.8 ppm (dd, $^{1}J_{PP}$ = 383, 372 Hz, P–I); *B* δ = −3.5 (t, $^{1}J_{PP}$ = 169 Hz, P–I), 10.2 ppm (d, $^{1}J_{PP}$ = 169 Hz, P–*t*Bu); MS (EI) *m/z*: 517.96 (2 %, M^+), 392.06 (9 %, $[M+H]^+-I$), 334.95 (25 %, $[M+H]^+-I-t$Bu), 278.92 (29 %, $[M+H]^+-I-t$Bu$-C_4H_8$), 96.99 (79 %, $(PH_2)_2P^+$), 56.97 (100 %, *t*Bu$^+$).

Synthesis of 5

To a stirred suspension of 0.11 g (2.9 mmol) $LiAlH_4$ in 20 mL Et_2O 1.24 g (2.9 mmol) Cl[3]Fc **3b** in 20 mL Et_2O were added slowly at room temperature. After continued stirring for 30 min all volatiles were removed under reduced pressure. The residue was extracted with 20 mL pentane and filtered off. From the resulting yellow solution the solvent was removed in vacuo. The resulting yellow crystalline product was spectroscopically pure. Recrystallization from pentane afforded crystals suitable for X-ray diffraction analysis. Yield: 1.10 g (97 %).

NMR spectra consist of signals from two diastereomers (*A* and *B*). ^{1}H NMR (400 MHz, C_6D_6): *A* δ = 1.22 (m, 18 H, *t*Bu CH_3), 3.86 (m, 2 H, Cp), 4.06 (m, 2 H, Cp), 4.17 (dt, $^{1}J_{HP}$ = 168 Hz, $^{2}J_{HP}$ = 7 Hz, P–H), 4.23 (m, 2 H, Cp), 4.54 ppm (m, 2 H, Cp); *B* δ = 1.22 (m, 18 H, *t*Bu CH_3), 3.49 (dt, $^{1}J_{HP}$ = 166 Hz, $^{2}J_{HP}$ = 8 Hz, P–H), 3.90 (m, 2 H, Cp), 4.07 (m, 2 H, Cp), 4.52 (m, 2 H, Cp), 4.58 ppm (m, 2 H, Cp); ^{13}C NMR (100 MHz, C_6D_6): *A* δ = 29.90 (m, *t*Bu CH_3), 30.61 (m, *t*Bu C_q), 69.42 (m, Cp), 72.67 (m, Cp), 72.20 (s, Cp), 74.80 (m, Cp C_{ipso}), 80.78 ppm (m, Cp); *B* δ = 29.71 (m, *t*Bu CH_3), 31.23 (m, *t*Bu C_q), 70.51 (m, Cp), 70.97 (m, Cp), 72.12 (s, Cp), 74.80 (m, Cp C_{ipso}), 80.12 ppm (m, Cp); ^{31}P{^{1}H} NMR (202 MHz, C_6D_6): *A* δ = −74.3 (dd, $^{1}J_{PP}$ = 295 Hz, $^{1}J_{PP}$ = 289 Hz, P–H), −9.8 (d, $^{1}J_{PP}$ = 294 Hz, P–*t*Bu), −9.8 ppm (d, $^{1}J_{PP}$ = 290 Hz, P–*t*Bu); *B* δ = −125.1 (t, $^{1}J_{PP}$ = 107 Hz, P–H), −6.5 ppm (d, $^{1}J_{PP}$ = 107 Hz, P–*t*Bu); MS (APCI) *m/z*: 392.0 (9 %, M^+), 393.1 (100 %, $[M+H]^+$).

Synthesis of 6

To a stirred mixture of 0.55 g (1.5 mmol) $Fe(C_5H_4PHtBu)_2$ **1** and 0.4 mL (2.5 mmol) TMEDA in 20 mL pentane 1.3 mL (3.3 mmol, 2.5 M) *n*BuLi solution in hexane were added dropwise at room temperature. After continued stirring for 1 h 0.52 g (3 mmol) $Cl_2P(NEt_2)$ were added dropwise to the orange suspension and stirred for another 30 min. All volatiles were removed under reduced pressure and the residue was extracted with 20 mL pentane and filtered off. The solvent was removed from the resulting orange solution in vacuo, yielding the crude product as orange solid which could not be satisfactorily separated from side products. Yield: 70 % crude product (from NMR spectra).

^{1}H NMR (400 MHz, C_6D_6): δ = 1.12 (m, 6 H, CH_3), 1.30 (m, 18 H, *t*Bu CH_3), 2.94 (m, 2 H, CH_2), 3.70 (m, 2 H, CH_2), 3.99 (m, 2 H, Cp), 4.07 (m, 2 H, Cp), 4.25 (m, 2 H, Cp), 4.43 ppm (m, 2 H, Cp); ^{13}C NMR (100 MHz, C_6D_6): δ = 15.26 (m, CH_3), 16.78 (m, CH_3), 30.69 (m, *t*Bu CH_3), 31.71 (m, *t*Bu C_q), 46.58 (m, CH_2), 48.94 (m, CH_2), 71.71 (m, Cp), 71.99 (m, Cp), 72.88 (m, Cp), 78.51 (m, Cp), 82.58 ppm (m, Cp C_{ipso}); ^{31}P{^{1}H} NMR (202 MHz, C_6D_6): δ = −16.3 (d, $^{1}J_{PP}$ = 168 Hz, P–*t*Bu), 70.0 ppm (t, $^{1}J_{PP}$ = 168 Hz, P–NEt_2); MS (EI) *m/z*: 463.34 (25 %, M^+), 392.27 (31 %, $[M+H]^+-NEt_2$), 279.10 (47 %, M^+−Fc), 335.19 (100 %, $[M+H]^+-NEt_2-t$Bu).

Synthesis of 7

A stirred solution of 1 g (2 mmol) $Fe(C_5H_4P(TMS)tBu)_2$ **4** and 0.314 g (2 mmol) *t*BuPCl_2 in 20 mL toluene was heated to reflux for 2 days. All volatiles were removed under reduced pressure to obtain product **4** as orange solid in near quantitative yields containing only minor traces of the P–P coupled $Fe(C_5H_4PtBu)_2$ as by-product. Recrystallization from diethylether afforded crystals suitable for X-ray diffraction analysis. Yield: 0.88 g (98 %).

^{1}H NMR (400 MHz, C_6D_6): δ = 1.39 (d, 18 H, $^{1}J_{HP}$ = 13 Hz, *t*Bu CH_3), 1.56 (d, 9 H, $^{1}J_{HP}$ = 13 Hz, *t*Bu CH_3), 3.99 (m, 2 H, Cp), 4.06 (m, 2 H, Cp), 4.24 (m, 2 H, Cp), 4.32 ppm (m, 2 H, Cp); ^{13}C NMR (100 MHz, C_6D_6): δ = 31.05 (m, 2C, *t*Bu CH_3), 31.05 (m, *t*Bu C_q), 31.76 (m, *t*Bu CH_3), 31.76 (m, *t*Bu C_q), 70.46 (m, Cp), 70.56 (s, Cp), 74.50 (m, Cp), 75.38 (m, Cp), 85.00 ppm (m, Cp C_{ipso}); ^{31}P{^{1}H} NMR (202 MHz, C_6D_6): δ = −10.4 (d, $^{1}J_{PP}$ = 357 Hz, P–*t*Bu), −10.3 (d, $^{1}J_{PP}$ = 356 Hz, P–*t*Bu), 46.2 ppm (dd, $^{1}J_{PP}$ = 356, 357 Hz, P–*t*Bu); MS (APCI) *m/z*: 449.137400 (100 %, $[M+H]^+$), 448.142052 (3 %, M^+).

Computational details

Quantum chemical calculations have been performed by the Gaussian 09 program package.[20] Full geometry optimization was performed for all the molecules at the B3LYP/6–311 + G** and the nature of the stationary point has been verified by a subsequent analysis of the second derivatives, which have been found all positive in case of minima, and exhibited a single negative value in case of transition states. For the visualization of the investigated molecules the program MOLDEN 4.0 was used.[21]

X-ray crystallography

X-ray diffraction measurements were performed on a Stoe IPDS 2 diffractometer (**7**) with an image plate detector and monochromated (graded multilayer mirror) Mo Kα radiation (Mo Genix) or on a Stoe StadiVari diffractometer with a Dectris Pilatus 200 K detector using either monochromated (plane graphite) Cu Kα (**5**) or Mo Kα (**3a**--**d**) radiation (Cu resp. Mo Genix). The data sets were recorded with ω-scans and corrected for Lorentz, polarization and absorption effects. The structures were solved using direct methods and refined without restraints by full-matrix least-squares techniques against F^2 (SHELXT and SHELXL-2014/7).[22] Details of the structure determinations and refinement for **3a**--**d**, **5** and **7** are summarized in Table S3 (see Supporting Information). Further programs used for analysis and visualization of structural information include WinGX and Mercury.[23]

CCDC 1545596, 1545597, 1545598, 1545599, 1545600, and 1545601 contain the supplementary crystallographic data for this paper. These data are provided free of charge by The Cambridge Crystallographic Data Centre.

Electrochemical measurements

Cyclic voltammetry and square wave measurements were carried out in a MBraun acrylic glovebox GB2202-C-VAC under inert argon atmosphere. All samples were measured in dichloromethane, which was dried over CaH, distilled and stored over molecular sieves (3 Å) under argon atmosphere. Tetrabutylammonium hexa-

fluorophosphate ([NBu_4][PF_6]) was used as the conducting salt with a concentration of 0.1 mol L^{-1}. The sample concentration during the measurements was set to 0.1 mmol L^{-1}. The setup consisted of a three-electrode cell with a platinum disk as working electrode, a silver spiral as counter electrode and a silver pseudo reference electrode. While the potential was driven on the WaveDriver 20 Bipotentiostat from Pine Research Instrumentation, electrochemical data were recorded via AfterMath (Ver. 1.2.5966; Pine Instruments). The half wave potentials of the redox processes were referenced using either ferrocene or decamethyl ferrocene and evaluated with OriginPro (Ver. 8.6.0; OriginLab Corporation).

Acknowledgements

The authors thank Prof. Gudat for helpful discussions and the Deutsche Forschungsgemeinschaft (PI 353/8-1 and PI 353/9-1) and OTKA NN 113772 within the framework of the ERA-Chemistry program for financial support. We also thank the EU-COST network CM1302 "Smart Inorganic Polymers" (SIPs) for funding an STSM.

Conflict of interest

The authors declare no conflict of interest.

Keywords: ab initio calculations · ferrocene · heteronuclear NMR spectroscopy · phosphorus · triphosphanes

[1] a) D. E. Herbert, U. F. J. Mayer, I. Manners, *Angew. Chem. Int. Ed.* **2007**, *46*, 5060 – 5081; b) I. Manners, U. Vogel in *Strained heteroatom-bridged metallocenophanes.*, (Ed. R. H. Gleiter, Henning), Wiley-VCH Verlag GmbH & Co. KGaA, Weinheim, Germany, **2004**, pp. 415 – 433; c) I. Manners, *Science* **2001**, *294*, 1664 – 1666; d) P. Nguyen, P. Gomez-Elipe, I. Manners, *Chem. Rev.* **1999**, *99*, 1515 – 1548; e) R. Pietschnig, *Chem. Soc. Rev.* **2016**, *45*, 5216 – 5231.

[2] a) C. Moser, F. Belaj, R. Pietschnig, *Chem. Eur. J.* **2009**, *15*, 12589 – 12591; b) Y. Tanimoto, Y. Ishizu, K. Kubo, K. Miyoshi, T. Mizuta, *J. Organomet. Chem.* **2012**, *713*, 80 – 88; c) C. Moser, F. Belaj, R. Pietschnig, *Phosphorus, Sulfur Silicon Relat. Elem.* **2015**, *190*, 837 – 844; d) Y. Maeno, Y. Ishizu, K. Kubo, S. Kume, T. Mizuta, *Dalton Trans.* **2016**, *45*, 19034 – 19044.

[3] H. R. Allcock, K. D. Lavin, G. H. Riding, P. R. Suszko, R. R. Whittle, *J. Am. Chem. Soc.* **1984**, *106*, 2337 – 2347.

[4] A. G. Osborne, H. M. Pain, M. B. Hursthouse, M. A. Mazid, *J. Organomet. Chem.* **1993**, *453*, 117 – 120.

[5] a) J. D. Masuda, A. J. Hoskin, T. W. Graham, C. Beddie, M. C. Fermin, N. Etkin, D. W. Stephan, *Chem. Eur. J.* **2006**, *12*, 8696 – 8707; b) A. J. Hoskin, D. W. Stephan, *Angew. Chem. Int. Ed.* **2001**, *40*, 1865 – 1867; *Angew. Chem.* **2001**, *113*, 1917 – 1919.

[6] D. Kargin, Z. Kelemen, K. Krekić, M. Maurer, C. Bruhn, L. Nyulászi, R. Pietschnig, *Dalton Trans.* **2016**, *45*, 2180 – 2189.

[7] a) H. J. Reich, R. R. Dykstra, *Organometallics* **1994**, *13*, 4578 – 4585; b) R. Wolf, A. Schisler, P. Lönnecke, C. Jones, E. Hey-Hawkins, *Eur. J. Inorg. Chem.* **2004**, *16*, 3277 – 3286.

[8] a) J. Hahn in *Phosphorus-31 NMR Spectroscopy in Stereochemical Analysis* (Eds.: J. G. Verkade, D. L. Quin), VCH Publishers, Deerfield Beach, FL, **1987**, 331 – 364; b) J. P. Albrand, H. Faucher, D. Gagnaire, J. B. Robert, *Chem. Phys. Lett.* **1976**, *38*, 521 – 523.

[9] a) R. E. Weston, *J. Am. Chem. Soc.* **1954**, *76*, 2645 – 2648; b) P. Schwerdtfeger, L. J. Laakkonen, P. Pyykkö, *J. Chem. Phys.* **1992**, *96*, 6807 – 6819.

[10] M. N. Glukhovtsev, A. Dransfeld, P. v. R. Schleyer, *J. Chem. Phys.* **1996**, *100*, 13447 – 13454.

[11] V. D. Romanenko, V. I. Tovstenko, L. N. Markovski, *Synthesis* **1980**, *1980*, 823 – 825.

[12] K. Issleib, W. Seidel, *Chem. Ber.* **1959**, *92*, 2681 – 2694.

[13] a) J. Bresien, K. Faust, A. Schulz, A. Villinger, *Angew. Chem. Int. Ed.* **2015**, *54*, 6926 – 6930; *Angew. Chem.* **2015**, *127*, 7030 – 7034; b) S. Burck, D. Gudat, M. Nieger, W.-W. Du Mont, *J. Am. Chem. Soc.* **2006**, *128*, 3946 – 3955; c) S. Weller, S. Schlindwein, R. Pietschnig, L. Nyulászi, D. Gudat, *Synthesis and Reactivity of 1,1′-Ferrocenyl-Diamino-Phosphane*, EWPC-14, Cluj-Napoca, Romania, **2017**, O10.

[14] R. T. Boeré, Y. Zhang, *J. Organomet. Chem.* **2005**, *690*, 2651 – 2657.

[15] P. Zanello, A. Cinquantini, M. Fontani, M. Giardiello, G. Giorgi, C. R. Landis, B. F. M. Kimmich, *J. Organomet. Chem.* **2001**, *637 – 639*, 800 – 804.

[16] O. J. Scherer, W. Gick, *Chem. Ber.* **1970**, *103*, 71 – 75.

[17] C. Moser, A. Orthaber, M. Nieger, F. Belaj, R. Pietschnig, *Dalton Trans.* **2006**, 3879 – 3885.

[18] M. Hillman, J. D. Austin, *Organometallics* **1987**, *6*, 1737 – 1743.

[19] N. J. Long, P. R. Raithby, P. Zanello, *Dalton Trans.* **1995**, 1245 – 1249.

[20] M. J. Frisch, G. W. Trucks, H. B. Schlegel, G. E. Scuseria, M. A. Robb, J. R. Cheeseman, G. Scalmani, V. Barone, B. Mennucci, G. A. Petersson, H. Nakatsuji, M. Caricato, X. Li, H. P. Hratchian, A. F. Izmaylov, J. Bloino, G. Zheng, J. L. Sonnenberg, M. Hada, M. Ehara, K. Toyota, R. Fukuda, J. Hasegawa, M. Ishida, T. Nakajima, Y. Honda, O. Kitao, H. Nakai, T. Vreven, J. Montgomery, J. A., J. E. Peralta, F. Ogliaro, M. Bearpark, J. J. Heyd, E. Brothers, K. N. Kudin, V. N. Staroverov, T. Keith, R. Kobayashi, J. Normand, K. Raghavachari, A. Rendell, J. C. Burant, S. S. Iyengar, J. Tomasi, M. Cossi, N. Rega, J. M. Millam, M. Klene, J. E. Knox, J. B. Cross, V. Bakken, C. Adamo, J. Jaramillo, R. Gomperts, R. E. Stratmann, O. Yazyev, A. J. Austin, R. Cammi, C. Pomelli, J. W. Ochterski, R. L. Martin, K. Morokuma, V. G. Zakrzewski, G. A. Voth, P. Salvador, J. J. Dannenberg, S. Dapprich, A. D. Daniels, O. Farkas, J. B. Foresman, J. V. Ortiz, J. Cioslowski, D. J. Fox *Gaussian 09*, *Revision B.01*, Gaussian Inc., Wallington CT, **2010**.

[21] G. Schaftenaar, J. H. Noordik, *J. Comput. Aided Mol. Des.* **2000**, *14*, 123 – 134.

[22] G. Sheldrick, *Acta Crystallogr. Sect. A* **2008**, *64*, 112 – 122.

[23] a) L. Farrugia, *J. Appl. Crystallogr.* **1999**, *32*, 837 – 838; b) C. F. Macrae, P. R. Edgington, P. McCabe, E. Pidcock, G. P. Shields, R. Taylor, M. Towler, J. van de Streek, *J. Appl. Crystallogr.* **2006**, *39*, 453 – 457.

Manuscript received: April 28, 2017
Accepted manuscript online: May 30, 2017
Version of record online: July 7, 2017

